Int. J. Electrochem. Sci., 11 **(2016)** 2550 - 2559

International Journal of
ELECTROCHEMICAL
SCIENCE
www.electrochemsci.org

Anthraquinone Immobilized on Reduced Graphene Oxide Sheets with Improved Electrochemical Properties for Supercapacitors

Jianli Ren, Xin Zhao[*]*, Junxian Zhang, and Qinghua Zhang*[*]

College of Materials Science & Engineering, State Key Laboratory for Modification of Chemical Fibers and Polymer Materials, Donghua University, Shanghai 201620, China
[*]E-mail: xzhao@dhu.edu.cn, qhzhang@dhu.edu.cn

Received: 22 December 2015 / *Accepted:* 7 February 2016 / *Published:* 1 March 2016

Organic compounds have attracted attention as inexpensive and environmentally friendly active materials for energy storage devices. To overcome their poor electrical conductivity and dissolublility in the electrolyte, the construction of electric conductive network to hold the organic molecules is necessary. Here, we selected reduced graphene oxide sheets as the conductive substrate and used hydrothermal reaction to immobilize 1,5-diaminoanthraquinone molecules on the graphene backbone. The obtained composite showed an improved specific capacitance with a specific capacitance of 277 F/g at scan rate of 5 mV/s, which was much larger than that of the pristine DAA (7.5 F/g) and RGO (63.3 F/g). Moreover, it also possessed a good cycling stability with a retention of 96.6% after 1000 cycles. The improved electrochemical behaviors of the composites are due to the conductive pathway of graphene and the positive synergistic effects between two components, indicating a great potential as electrodes for supercapacitors.

Keywords: anthraquinone, graphene oxide, electrochemical, supercapacitors

1. INTRODUCTION

Supercapacitors (SCs), a new type of energy storage equipment, have received a worldwide attention because of their high power density, long cycle life and low maintenance.[1, 2] According to the storage mechanisms, SCs could be classified into two types: electrical double-layer capacitors (EDLCs) and pseudocapacitors. The capacitance of EDLCs comes from the charge accumulation at the electrode/electrolyte interface and carbon based materials with large surface areas are used as electrodes.[3] While the capacitance of pseudocapacitors is due to the fast reversible faradic transitions of electro-active species of the electrode, such as transition metal oxides and conducting polymers, etc.

Apparently, the strategy of introducing redox materials into carbonaceous materials provides a chance to merge the merits of these two kinds of electrodes, which can effectively enhance the capacitance performance of supercapacitors. Therefore, recent efforts on electrode materials have been devoted on fabricating composite materials, such as carbon/transition metal oxides[4-8] and carbon conducting polymers,[9-13] etc.

Apart from conducting polymers and transition metal oxides, there are some organic molecules with reversible electrochemical redox couples that could produce pseudocapacitance, such like anthraquinones,[14-16] benzoquinone,[17, 18] organosulfurs[19, 20] and so on. As one of the redox-active small organic molecules, anthraquinones (AQ) are expected to possess considerable charge storage capacities beyond conventional redox-active metal oxides, primarily owing to the multi-electron reactions in a low-molecular-weight. However, the electrical insulation and the instability of small molecules are limited for its applications as electrodes for SCs. To fully realize their pseudocapacitance, they are commonly attached on conductive substrates such as active carbon, carbon nanotubes, templated carbon, carbon fiber and graphene,[21-28] etc.

For instance, Duan *et al*. introduced hydroquinone into high-surface-area 3D graphene framework via π-π interactions, and the as-prepared functionalized graphene hydrogels showed an high specific capacitance of 441 F/g in 1 M H2SO4 aqueous electrolyte.[29] Hu *et al.* introduced reversible redox couples (anthraquinone/ anthracenol) onto graphene framework, and the composite exhibited a high specific capacitance of 396 F/g at 1 A/g and a 97% retention after 2000 cycles due to π-π stacking interaction between anthraquinone molecules and graphene network. They also fabricated an asymmetric supercapcitors using graphene and anthraquinone/graphene framework as electrodes, of which the potential window could be extended to 1.6 V, and energy density could reach to 13.2 Wh/kg.[30] Campbell et al. developed an anthraquinone-modified graphene macro-assemblies hybrid battery/supercapacitor, which had a 2.9 times increased electrical energy storage capacity compared with the untreated graphene macro-assemblies.[31] Pickup and coworkers used anthraquinone modified carbon fabric and unmodified carbon fabrics with Nafion as separator in 1 M sulfuric acid to fabricate an asymmetric supercapacitor, which showed an 40% higher average capacitance and 56-86% higher energy density than unmodified carbon fabric.[32] And they also used other materials as positive electrodes, all of them exhibited excellent electrochemical performance.[33, 34] Shi et al. introduced 2-aminoanthraquione into chemically modified graphene, and the composite showed a high specific capacitance of 258 F/g at 0.3 A/g, higher than that of the pure graphene hydrogel (193 F/g), and they also have an excellent rate capability and a long cycle life.[15] Besides, Chen et al. incorporated anthraquinone(AQ) with hierarchical porous carbon nanotubes (HPCNTs), and the composite exhibited a ultrahigh specific capacitance of 710 F/g when mass ratio of AQ/HPCNTs is 7/5, while the unmodified HPCNTs was only 304 F/g at 1 A/g.[35] All of the reports demonstrated that small molecules with redox active groups are useful to improve the capacitance of the electrode when combining with carbon materials.

In this work, small organic molecule, 1,5-diaminoanthraquione (DAA), was immobilized on the sheets of reduced graphene oxide (RGO) by the π-π interactions between the conjugated carbonyl groups on DAA and RGO. Thanks to the conductive network provided by graphene sheets, the composites with DAA supported on graphene showed an improved specific capacitance in comparison

with that of pristine DAA in 1 M H2SO4. Furthermore, it also showed a specific capacitance of 91.5 F/g at 2 A/g and possessed a good cycling stability (retention of 96.6% after 1000 cycles). The improved electrochemical behaviors of the composites suggest its great potential as electrodes for supercapacitors.

2. EXPERIMENTAL WORK

2.1. Synthesis of RGO/DAA

A certain amount of DAA was dissolved in 50 mL dimethylformamide (DMF) and stirred vigorously. 0.1 g graphite oxide was dissolved in 20 mL DMF and was added into the above solution. Then the mixed solution was sonicated for 1 h, then continued to stir 2 h to get a well dispersed solution. Finally, the homogeneous dispersion was transferred into a stainless steel autoclave, and reacted at 180 ℃ for 12 h. When the reaction finished, the products were washed by deionized water and reduced by hydriodic acid to get the final products. The obtained samples were designated here as RGO/DAA (x:y) composites. The feeding amounts of DAA were 0.01 g, 0.02 g, 0.14 g, 0.5 g for the samples RGO/DAA(10:1), (5:1), (5:7), (1:5), respectively.

2.2. Characterization

The morphologies of DAA, RGO and RGO/DAA were investigated by field emission electron microscopy (FESEM; Hitachi S-4800). The nitrogen adsorption-desorption isotherms were measured at 77 K by an automatic adsorption instrument (ASAP 2020, Micromeritics). Element Analysis was carried out using an Elmentar Vario EL III Elemental Analyzer. Fourier Transform Infrared (FT-IR) spectra were tested on Nicolet 8700 (Thermal Fisher). Raman spectra were collected using a 633 nm laser with RM 100 under ambient condition (Renishaw Plc, invia Reflex). X-ray diffraction (XRD) patterns were obtained by using a Rigaku D/max-2550 PC X-ray diffractometer with Cu Kα radiation.

2.3. Electrochemical Measurement

The electrochemical capacitive behaviors of the electrodes were tested on an Autolab electrochemical workstation (Metrohm, Switzerland). The working electrodes were fabricated by mixing 75 wt% active materials, 20 wt% acetylene black and 5 wt% polytetrafluoroethylene (PTFE) together to get a homogenous mixture. Then the mixture was pressed into slice, with the extra solvent evaporated at 60℃. The tests were carried out by a three electrode system in 1 M H_2SO_4 solution with a saturated calomel electrode (SCE) as the reference electrode and a platinum electrode as the counter electrode. Cyclic Voltammetry (CV) was measured at different scan rates varying from 5 mV/s to 100 mV/s, and galvanostatic charge-discharge studies were performed between 0 V to 0.8 V at various current densities, and electrochemical impedance spectroscopy (EIS) measurements were tested over

the frequency range from 100 kHz to 0.01 Hz at an AC voltage with 5 mV amplitude. Finally, the cycle-life stability tests were carried out between 0 V and 0.8 V (vs. SCE) at a current density of 2 A/g for 1000 cycles. The specific capacitance can be calculated from the following equation: $C = \frac{i}{mv}$, Where i is the current, m is the mass of active material, v is scan rate. The specific capacitance of electrode materials based on galvanostatic charge/discharge curves was calculated from the following equation: $C = \frac{It}{m\Delta V}$,Where I is the discharge current, t is the discharge time, m is the mass of active material, ΔV is the applied potential window.

3. RESULTS AND DISCUSSION

The fabrication process for RGO/DAA composites is illustrated in Figure 1. DAA molecules could be adsorbed on the surface of GO by π-π interactions between the conjugated carbonyl groups on DAA and graphene and covalently immobilized on the graphene sheets by hydrothermal reaction. To confirm the high conductivity of graphene substrate, GO was reduced by hydriodic acid to obtain the composite with DAA anchored on RGO. In this design, the aromatic ring of DAA is inclined to connect between the sp2 network of graphene sheets, which results in a fast redox reaction of DAA due to the low charge transfer resistance.[30]

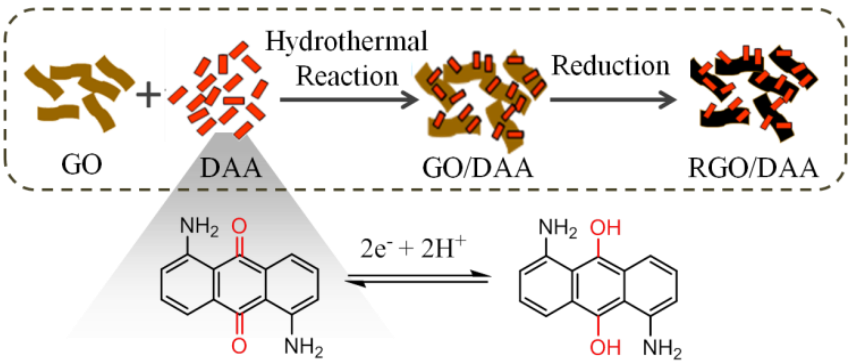

Figure 1. Schematic diagram for the preparation of RGO/DAA

The morphologies of as-prepared RGO/DAA composites were shown in Figure 2. From the SEM images, it can be seen that the samples with various DAA contents displayed the similar morphologies, which have an interconnected 3D framework and pore walls consisting of ultrathin layers of stacked graphene sheets. It indicates that the additional of DAA had little influence on the structures of RGO. Although it is hardly to identify the morphologies of DAA molecules from the images, the results of elemental analysis of RGO/DAA samples show an higher N content (2.8 wt % for RGO/DAA(1:5)) than that of RGO (0.45 wt%), indicating the existence of DAA. Besides, the results of structural analysis below also could confirm that DAA molecules have been successfully attached on the sheets of RGO.

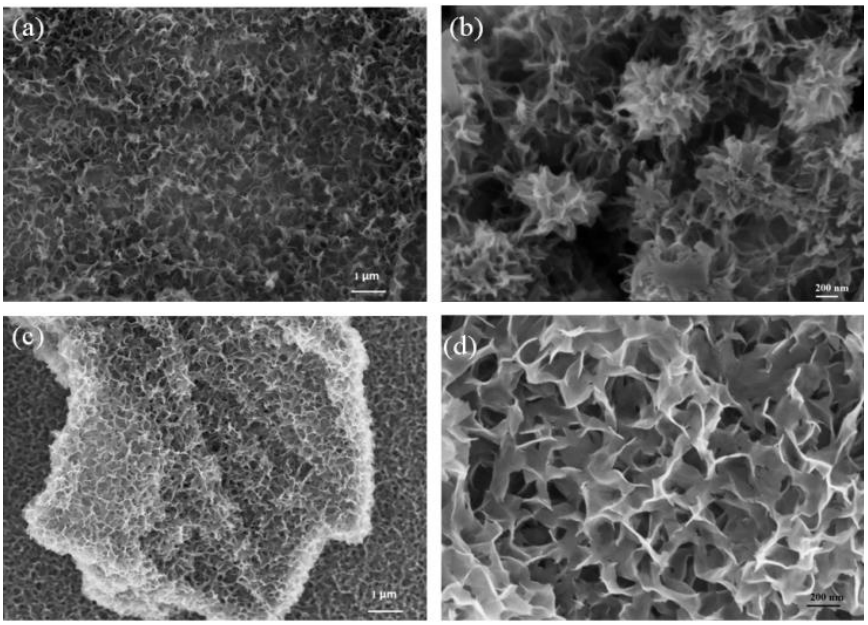

Figure 2. FE-SEM images of different ratio of RGO/DAA. (a) RGO/DAA(1:5), (b) RGO/DAA(5:7), (c) and (d) RGO/DAA(5:1)

The FTIR spectra of DAA and various RGO/DAA samples are illustrated in Figure 3 (a). Two peaks at approximately 3420 and 3315 cm^{-1} in the spectrum of DAA monomer can be ascribed to the NH_2 stretching on its aromatic ring. Several more characteristic peaks for DAA also could be observed at 1614, 1544, 1277 and 495 cm^{-1}, corresponding to C=O stretching, the anthraquinone ring, C-N stretching, and C-C-NH_2 band in DAA, respectively. For the RGO/DAA hybrids, it is interesting to observe that the strong two signals of NH_2 stretching for DAA are displaced by a broad single peak around 3440 cm^{-1}, which could be assigned to the NH groups like in the structure of poly(1,5-diaminoanthraquinone).[36] And the adsorption at 495 cm^{-1} becomes much weaker in the spectra of RGO/DAA samples.[37] This indicates that a large amount of free NH_2 groups has changed into NH groups in RGO/DAA, confirming the successful covalently attachment of DAA molecules on graphene sheets. Besides, the peaks at 1544 and 1277 cm^{-1} of DAA also could be noticed for RGO/DAA and the signals become more obvious with the increase of DAA loading, suggesting the existence of DAA molecules. The band for C=O stretching of DAA at 1614 cm^{-1} might be overlapped by the C=C stretching of graphene in the structure of RGO /DAA at ca. 1605 cm^{-1}. [38]

The XRD patterns of the samples are shown in Figure 3 (b). The pattern of DAA shows several sharp peaks, which indicates the highly crystalline structure of DAA small molecules. However, after hydrothermal reaction, the traces of RGO/DAA consist mainly of a broad (002) signal at around 25.7°, suggesting the amorphous structure of the obtained composites. Compared with the RGO, the (002) peak of RGO/DAA shifts from 24.5° to 25.7°, indicating a decrease in the layer spaces of the composites. Additionally, the peak intensity for RGO/DAA increase relatively. These results might be caused by the covalent linkage of DAA organic molecules between graphene layers and the recovery of the conjugated system for graphene sheets after the hydrothermal reaction.

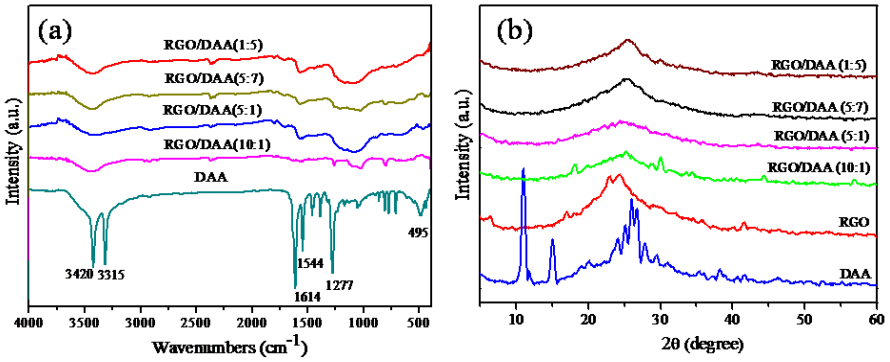

Figure 3. FTIR spectra (a) and XRD pattern (b) of DAA, RGO and different ratio of RGO/DAA

As shown in Figure 4 (a), nitrogen adsorption-desorption isotherm of RGO/DAA(5:1) shows a type IV hysteresis loop which is similar to that of RGO, illustrating a characteristic mesoporous feature. The total pore volume of RGO/DAA increases to 0.048 cm^3/g compared to that of RGO (0.007 cm^3/g) and the specific surface area of RGO/DAA (32.5 m^2/g) is much larger than that of RGO (3.2 m^2/g), indicating the improved porous structure after the attachment of DAA on RGO. Furthermore, the obtained RGO/DAA hybrids were also analyzed by Raman spectroscopy.

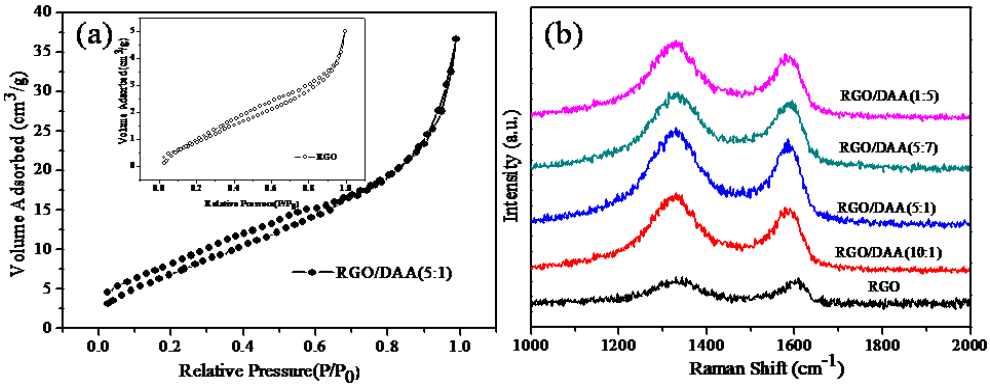

Figure 4. Nitrogen adsorption-desorption isotherms of RGO/DAA (5:1) (a) and RGO (inset of (a)) and Raman spectra of RGO and different ratio of RGO/DAA (b)

As illustrated in Figure 4 (b), Raman spectra of RGO and all of the RGO/DAA show the band around 1340 and 1600 cm^{-1}, corresponding to the D and G band of graphite carbon, respectively. The intensity ratio between the D-band and G-band (I_D/I_G) for RGO/DAA remains the same value for RGO/DAA (ranging from 1.10 to 1.19) and RGO (1.05), suggesting the well-maintained structure of graphene which could provide a good conductive pathway and facilitate electron transfer inside the electrode.

The electrochemical performances of RGO/DAA composites with various DAA loadings were measured by cyclic voltammetry and galvanostatic charge/discharge tests by a three-electrode system in 1 M H_2SO_4. Figure 5 shows the CV curves of DAA and RGO/DAA(5:1) at different scan rates. It is obvious to observe a pair of redox peaks for DAA (Figure 5 (a)), indicating the presence of faradaic

capacitance originated from the redox active groups. When increasing the scan rate, the anodic peaks shift to a higher potential, while the cathodic peaks turn to lower potential, the phenomenon of increasing peak separation reveals a poor reversibility of DAA. Figure 5 (b) gives the CV curve of RGO/DAA(5:1). Compared with other anthraquinone-modified carbon materials,[30, 31] the overall shape of the curves are quasi-rectangle but the redox peaks of DAA could be seen in a slow scan rate. With the increasing scan rate, the redox peaks are hardly to be seen, which may be caused by the fast diffusion of electrolyte ions who have not enough time to carry on redox reaction. Figure 5 (c) shows the CV curves of DAA, RGO, RGO/DAA(10:1), (5:1), (5:7), (1:5) electrodes in the potential range from -0.2 to 0.8 V at a scan rate of 5 mV/ s. Obviously, the specific capacitance of composite electrodes are higher than that of RGO and DAA, which combines both double layer capacitance and faradaic capacitance. Furthermore, the CV curve for RGO/DAA(5:1) shows the largest area, indicating its larger capacitance than that of others. Figure 5 (d) displays the calculated specific capacitances for various samples. The specific capacitance of DAA, RGO, RGO/ DAA(10:1), (5:1), (5:7), (1:5) were 7.5, 63.3, 152.8, 277.5, 148,4, 118 F/g at 5 mV/ s, respectively. RGO/DAA(5:1) showed the highest value and was much larger than that of the pristine DAA and RGO.

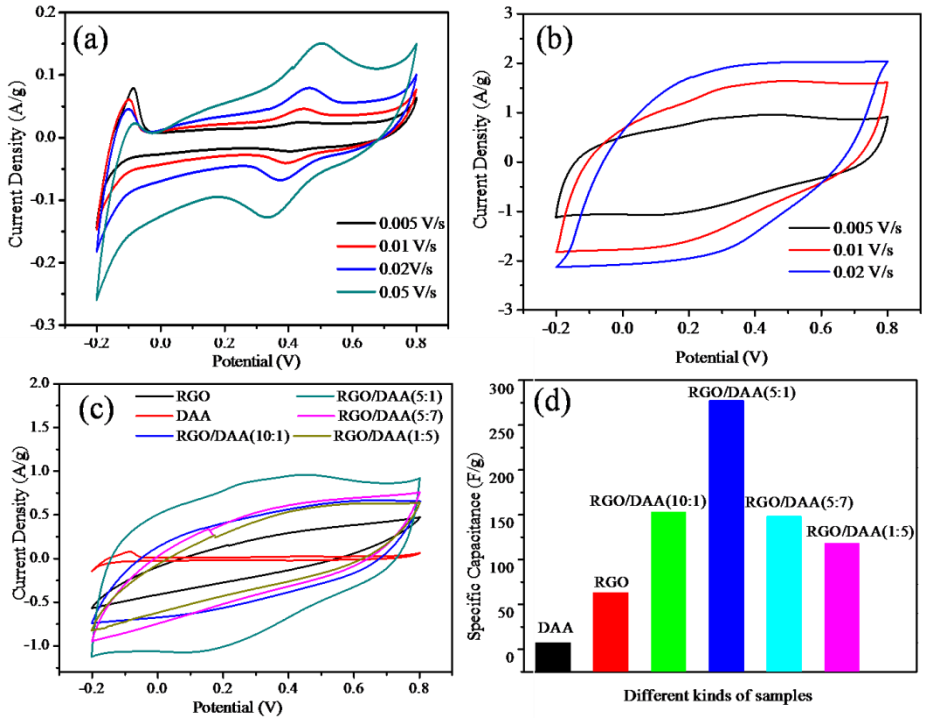

Figure 5. CV curves of (a) DAA and (b) RGO/DAA(5:1) at different scan rates, (c) CV curves of different samples at a scan rate of 5 mV/s, (d) specific capacitance of different samples.

Figure 6 (a) presents the galvanostatic charge-discharge curves for the composites with different ratio of RGO and DAA at current density of 2 A/g. Obviously, the charging and discharging time of composites are longer than those of DAA and RGO, which could be ascribed to the combination of EDLC and Faradaic capacitance. The specific capacitance of DAA, RGO, RGO/

DAA(10:1), (5:1), (5:7), (1:5) was calculated to be 2.3, 134.7, 136, 195.9, 167.5, 164.3 F/g at 0.1 A/g, respectively. Compared with RGO, there is a 45% improvement of specific capacitance in RGO/DAA(5:1), which is higher than the anthraquinone modified graphene.[15] The improved capacitance for the composites could be attributed to the synergistic effects between RGO and DAA and the high conductivity of RGO could facilitate electron transfer inside the electrode and shorten the ion diffusion pathway to the active materials.[30, 39] Interestingly, when the feeding ratio of RGO and DAA is 5:1, the as-prepared composite shows the highest specific capacitance. This result may be due to the blocked electron transfer and ion diffusion path caused by too much DAA addition, which is not beneficial for electrolyte ions to be adsorbed on the active groups. The rate performance of various samples with different current density is illustrated in Figure 6 (b), the specific capacitance decreases with current density increasing from 0.1 A/g to 2 A/g. The RGO/ DAA(5:1) shows retention of 47% specific capacitance after current density change from 0.1 A/g to 2 A/g, higher than other composites and DAA monomer . Electrochemical impedance tests were also carried out at the frequency from 0.01 Hz to 100 kHz, and typical Nyquist plot of RGO, DAA and different ratio of RGO/DAA are displayed in Figure 6 (c). Obviously, each spectrum includes two parts: a semicircle in the high-frequency and a line in the low-frequency. The diameter of the semicircle is corresponding to the charge-transfer resistance of the device. As shown in the inset of the Figure 6 (c), the semicircle of RGO/ DAA(5:1) is the smallest (10.5 ohm), which indicates that suitable addition of DAA is favorable to remain the conductive pathway of RGO sheets and improve the charge transfer, which is consistent with charge-discharge curves. At the same time, in the low-frequency region, the slope of RGO/DAA(5:1) displays large slope than that of others, which reveals a better capacitive characteristic of the composite.

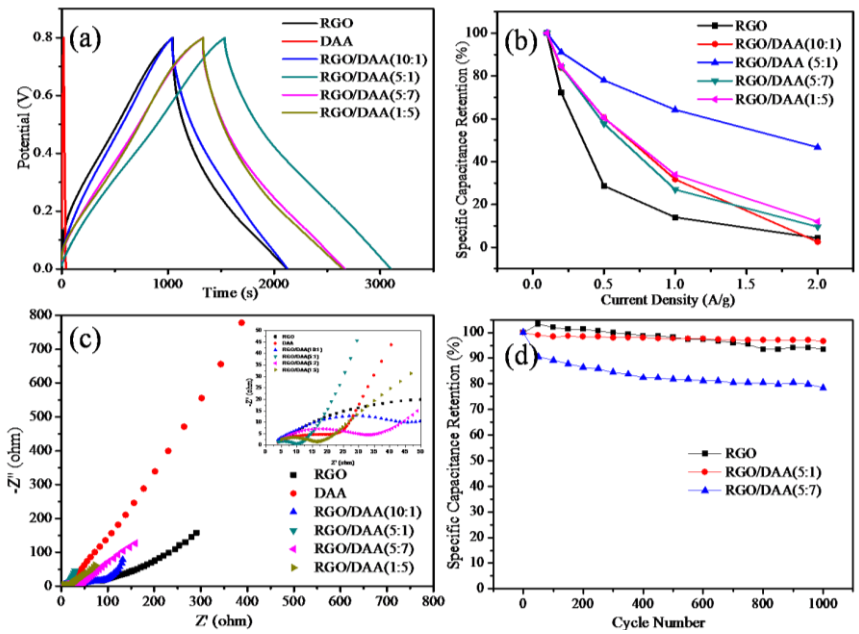

Figure 6. Electrochemical performance of DAA, RGO and RGO/DAA with different ratios. (a) Galvanostatic charge/discharge curves at a current density of 0.1 A/g (b) The specific capacitance as a function of various current densities (c) Nyquist plots at the frequency range of 10^{5}-10^{-2} Hz; (d) cycling performance of RGO/DAA (5:1), RGO/ DAA(5:7) and RGO at a current density of 2 A/g

Furethermore, the cycle tests of RGO, RGO/DAA(5:1) and RGO/DAA(5:7) were also measured at a current density of 2 A/g as shown in Figure 6 (d). After 1000 cycles, the retention of specific capacitance of three samples are 93.4, 96.6 and 78.4% for RGO, RGO/DAA(5:1) and RGO/DAA(5:7), respectively. The high retention of specific capacitance of RGO/DAA(5:1) is comparable to other anthraquinone/carbon nanotube composite,[35] showing the fact that there is no sacrifice of stability of the material with the addition of DAA. It is suggested that a reasonable loading of DAA organic small molecular could not only increase the specific capacitance but also benefit to improve the cycling performance, indicating that a stable microstructure during the charge-discharge repeating process. When the content of DAA increases, some part of small molecule might dissolve during the charge-discharge process, leading to a declined performance. Moreover, the cycling curves of RGO/DAA(5:7) showed an obvious drop in the first 50 cycles, indicating an unstable structure with too more DAA loading in the composites.

4. CONCULSIONS

In conclusion, we have demonstrated a hydrothermal reaction to immobilize DAA on the RGO substrate, the addition of DAA as a redox modifier for the electrode material has been shown to give a great promotion in specific capacitance compared with RGO and DAA, respectively. After DAA modification, the composites also exhibit excellent rate capability and cycle performance, which are generated by the DAA-RGO π-π stacking interactions and DAA-DAA π-π stacking interactions. The good electrochemical performances of the composite indicate its potential as electrode for supercapacitors.

ACKNOWLEDGEMENTS
The This work was financially supported by the National Natural Science foundation of China (51403036), Shanghai Education Commission (14YF1405300), Shanghai Education development foundation (14S10656), Specialized Research Fund for the Doctoral Program of Higher Education of China (SRFDP 20130075120018) and Fundamental Research Funds for the Central University (2232014D3-09).

References

1. C. Liu, F. Li, L.-P. Ma and H.-M. Cheng, *Advanced materials*, 22 (2010) E28
2. L. L. Zhang and X. S. Zhao, *Chemical Society Reviews*, 38 (2009) 2520
3. P. Simon and Y. Gogotsi, *Nature Materials*, 7 (2008) 845
4. J. L. Yin and J. Y. Park, *Journal of Solid State Electrochemistry*, 19 (2015) 2391
5. A. Choudhury, J. S. Bonso, M. Wunch, K. S. Yang, J. P. Ferraris and D. J. Yang, *Journal of Power Sources*, 287 (2015) 283
6. S. Ullah, I. A. Khan, M. Choucair, A. Badshah, I. Khan and M. A. Nadeem, *Electrochimica Acta*, 171 (2015) 142
7. D. H. Fam, S. Azoubel, L. Liu, J. Huang, D. Mandler, S. Magdassi and A. Y. Tok, *Journal of Materials Science*, 50 (2015) 6578

8. Y.-H. Li, Q.-Y. Li, H.-Q. Wang, Y.-G. Huang, X.-H. Zhang, Q. Wu, H.-Q. Gao and J.-H. Yang, *Applied Energy*, 153 (2015) 78
9. K. Lota, G. Lota, A. Sierczynska and I. Acznik, *Synthetic Metals*, 203 (2015) 44
10. C. Tran, R. Singhal, D. Lawrence and V. Kalra, *Journal of Power Sources*, 293 (2015) 373
11. W. Yang, J. Xu, Y. Yang, Y. Chen, Y. Zhao, S. Li and Y. Jiang, *J Mater Sci: Mater Electron*, 26 (2015) 1668
12. A. Olad and H. Gharekhani, *Progress in Organic Coatings*, 81 (2015) 19
13. P. Yu, Y. Li, X. Zhao, L. Wu and Q. Zhang, *Langmuir : the ACS journal of surfaces and colloids*, 30 (2014) 5306
14. N. An, Y. An, Z. Hu, Y. Zhang, Y. Yang and Z. Lei, *RSC Advances*, 5 (2015) 63624
15. Q. Wu, Y. Sun, H. Bai and G. Shi, *Physical chemistry chemical physics : PCCP*, 13 (2011) 11193
16. G. Pognon, T. Brousse, L. Demarconnay and D. Bélanger, *Journal of Power Sources*, 196 (2011) 4117
17. C. Singh and A. Paul, *The Journal of Physical Chemistry C*, 119 (2015) 11382
18. Eacute, A. Ndez, S. Isikli, uuml, heda, Iacute, R. Az and uuml, *Electrochemistry*, 81 (2013) 853
19. K. Naoi, K. i. Kawase and Y. Inoue, *Journal of The Electrochemical Society*, 144 (1997) L170
20. S. J. Visco, C. C. Mailhe, L. C. De Jonghe and M. B. Armand, *Journal of The Electrochemical Society*, 136 (1989) 661
21. H. Cui, J. Zheng, Y. Zhu, Z. Wang, S. Jia and Z. Zhu, *Journal of Power Sources*, 293 (2015) 143
22. H.-C. Hsu, C.-H. Wang, Y.-C. Chang, J.-H. Hu, B.-Y. Yao and C.-Y. Lin, *Journal of Physics and Chemistry of Solids*, 85 (2015) 62
23. B. Lobato, V. Vretenár, P. Kotrusz, M. Hulman and T. A. Centeno, *Journal of Colloid and Interface Science*, 446 (2015) 203
24. C. Ma, Y. Song, J. Shi, D. Zhang, X. Zhai, M. Zhong, Q. Guo and L. Liu, *Carbon*, 51 (2013) 290
25. C. Tran and V. Kalra, *Journal of Power Sources*, 235 (2013) 289
26. Z. Wang, Z. Wu, G. Di Benedetto, J. L. Zunino Iii and S. Mitra, *Carbon*, 91 (2015) 103
27. D. H. Seo, S. Yick, D. Su, G. Wang, Z. J. Han and K. Ostrikov, *Carbon*, 91 (2015) 386
28. G. Nystrom, A. Marais, E. Karabulut, L. Wagberg, Y. Cui and M. M. Hamedi, *Nat Commun*, 6 (2015
29. Y. Xu, Z. Lin, X. Huang, Y. Wang, Y. Huang and X. Duan, *Advanced materials*, 25 (2013) 5779
30. N. An, F. Zhang, Z. Hu, Z. Li, L. Li, Y. Yang, B. Guo and Z. Lei, *RSC Advances*, 5 (2015) 23942
31. P. G. Campbell, M. D. Merrill, B. C. Wood, E. Montalvo, M. A. Worsley, T. F. Baumann and J. Biener, *Journal of Materials Chemistry A*, 2 (2014) 17764
32. K. Kalinathan, D. P. DesRoches, X. Liu and P. G. Pickup, *Journal of Power Sources*, 181 (2008) 182
33. Z. Algharaibeh, X. Liu and P. G. Pickup, *Journal of Power Sources*, 187 (2009) 640
34. Z. Algharaibeh and P. G. Pickup, *Electrochemistry Communications*, 13 (2011) 147
35. X. Chen, H. Wang, H. Yi, X. Wang, X. Yan and Z. Guo, *The Journal of Physical Chemistry C*, 118 (2014) 8262
36. X. G. Li, H. Li and M. R. Huang, *Chemistry – A European Journal*, 13 (2007) 8884
37. R. Gottam and P. Srinivasan, *Journal of Applied Polymer Science*, 132 (2015) n/a
38. M. Sun, Q. Tang, T. Zhang and G. Wang, *RSC Advances*, 4 (2014) 7774
39. H. Wang, H. Yi, C. Zhu, X. Wang and H. Jin Fan, *Nano Energy*, 13 (2015) 658